

Efficiency Enhancement of Organic Solar Cells Using Hydrophobic Antireflective Inverted Moth-Eye Nanopatterned PDMS Films

Jung Woo Leem, Sehwan Kim, Soo Hyun Lee, John A. Rogers, Eunkyong Kim,* and Jae Su Yu*

Poly-dimethylsiloxane (PDMS) films with 2D periodic inverted moth-eye nanopatterns on one surface are implemented as antireflection (AR) layers on a glass substrate for efficient light capture in encapsulated organic solar cells (OSCs). The inverted moth-eye nanopatterned PDMS (IMN PDMS) films are fabricated by a soft imprint lithographic method using conical subwavelength grating patterns formed by laser interference lithography/dry etching. Their optical characteristics, together with theoretical analysis using rigorous coupled-wave analysis simulation, and wetting behaviors are investigated. For a period of 380 nm, IMN PDMS films laminated on glass substrates exhibit a hydrophobic surface with a water contact angle (θ_{CA}) of $\approx 120^\circ$ and solar weighted transmittance (SWT) of $\approx 94.2\%$, both significantly higher than those ($\theta_{CA} \approx 36^\circ$ and $SWT \approx 90.3\%$) of bare glass substrates. By employing IMN PDMS films with a period of 380 nm on glass substrates for OSCs, an enhanced power conversion efficiency (PCE) of 6.19% is obtained mainly due to the increased short-circuit current density (J_{sc}) of 19.74 mA cm^{-2} compared to the OSCs with the bare glass substrates (PCE = 5.16% and $J_{sc} = 17.25 \text{ mA cm}^{-2}$). For the OSCs, the device stability is also studied.

1. Introduction

There is increasing interest in organic solar cells (OSCs) based on conjugated polymers due to their promising potential for future energy sources with low cost, high throughput, light weight, and superior mechanical flexibility.^[1–3] Recently, Heliateck in Germany demonstrated an OSC with a power

conversion efficiency (PCE) of 12%, which represents the current world-record value for OSCs.^[4] However, this value is much lower compared to inorganic multi-junction solar cells, where PCE can exceed 40%.^[5] Thus, further improvements in PCEs of OSCs appear possible. Among various strategies for increasing PCE, one simple approach is to enhance the light collection and trapping in the active layer of OSCs.^[6–10] For this purpose, high-efficiency broadband antireflection (AR) coatings are required on externally facing surfaces of the transparent superstrates (i.e., glasses or plastics), to suppress Fresnel surface reflections.^[11] Soft imprint lithographic methods have been used to create nanopatterned AR films in flexible and stretchable polymer-based materials including poly-dimethylsiloxane (PDMS), polycarbonate, polymethyl methacrylate (PMMA), and polyurethane.^[12–15] Such techniques are compatible with continuous processing, which is advantageous for simple, low-cost, and high-throughput production without the need for costly high-vacuum equipment.^[16] Also, the resulting films can be repeatedly used as elastomeric stamps, membranes, or substrates as well as protective layers against mechanical damage to the underlying devices.^[17–21] Although there are several published studies on AR nanostructures in polymer films (i.e., PDMS^[22] and PMMA^[23]) for OSCs, there is little work on the use of the elastomeric PDMS films with inverted moth-eye nanopatterns. Separately, self-cleaning properties have been found to be useful in removing any surface dirt or dust particles for device applications.^[24] Thus, the wetting behaviors of inverted moth-eye nanopatterned PDMS (IMN PDMS) are also relevant. Here, we fabricate IMN PDMS films by soft imprint lithography using silicon (Si) masters of periodic arrays with conical subwavelength grating patterns. Their wettability and optical properties, together with results of rigorous coupled-wave analysis (RCWA) simulation, on glass substrates are investigated. By laminating the IMN PDMS films as AR layers on glass substrates of encapsulated OSCs, the effects on device characteristics including their stability are also studied.

J. W. Leem, S. H. Lee, Prof. J. S. Yu
Department of Electronics and Radio Engineering
Kyung Hee University
1 Seocheon-dong, Giheung-gu, Yongin-si,
Gyeonggi-do, 446–701, Korea
E-mail: jsyu@khu.ac.kr

S. Kim, Prof. E. Kim
Department of Chemical and Biomolecular Engineering
Yonsei University
50 Yonsei-ro, Seodaemun-gu, Seoul 120–749, Korea
E-mail: eunkim@yonsei.ac.kr

Prof. J. A. Rogers
Department of Materials Science and Engineering
University of Illinois at Urbana-Champaign
Urbana, IL 61801, USA



DOI: 10.1002/aenm.201301315

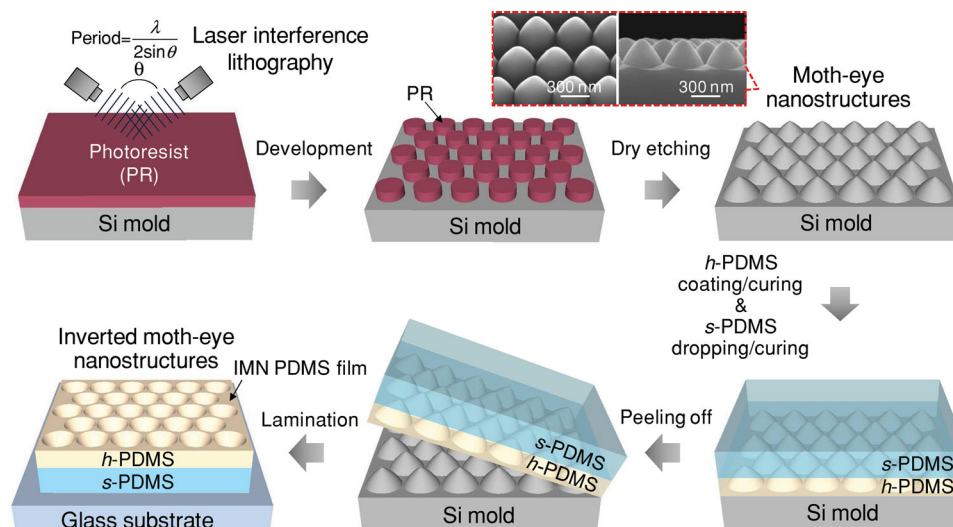


Figure 1. Schematic illustration of process steps for the fabrication of inverted moth-eye nanostructures (IMN) on one side of PDMS films by the soft imprint lithography using a Si master. The IMN PDMS film serves as an AR layer when laminated on glass substrate. SEM images of the Si master with periodic conical subwavelength grating arrays (i.e., moth-eye nanostructures) for a period of 380 nm are also shown.

2. Results and Discussion

Figure 1 shows a schematic illustration of process steps for the fabrication of inverted moth-eye nanostructures on one side of PDMS films by the soft imprint lithography using a Si master. These masters consist of 2D periodic hexagonal array patterns of closely packed conical subwavelength grating structures (i.e., moth-eye nanostructures), as shown in the scanning electron microscopy (SEM) images of **Figure 1**. Periods of 380, 500, and 650 nm were prepared by using laser interference lithography and dry etching processes. To prevent deformation and distortion of the replicated features, a hard PDMS (*h*-PDMS) solution was spin-casted onto the master and then cured. A soft PDMS (*s*-PDMS) layer, formed by casting and curing a prepolymer on the *h*-PDMS/Si, enables manual application and intimate conformable contact on flat surfaces, in a non-destructive and reversible manner. The PDMS (*h*-PDMS/*s*-PDMS) films were peeled off from the Si master mold, thus creating a PDMS film with inverted moth-eye nanostructures (i.e., IMN PDMS film). Films with thicknesses of $\approx 250 \mu\text{m}$ were used with soda lime glass substrates.

Figure 2a shows 30°-tilted oblique- and side-view SEM images of the flat PDMS film and IMN PDMS films with different periods (*P*) of 380, 500, and 650 nm and **Figure 2b** shows photographs of a water droplet on the corresponding samples. For the bare glass substrate, a photograph of a water droplet is also shown in **Figure 2b**. The flat PDMS film was formed using a flat Si master. As shown in **Figure 2a**, inverted moth-eye nanopatterns with 2D periodic hexagonal symmetry as well as the flat pattern were well formed on the surfaces of *h*-PDMS/*s*-PDMS films. The inverted moth-eye nanopatterns had depths of 250, 300, and 360 nm for periods of 380, 500, and 650 nm (i.e., P380, P500, and P650), respectively. To compare with the case of *h*-PDMS, for the period of 380 nm, inverted moth-eye nanostructures were also fabricated using only

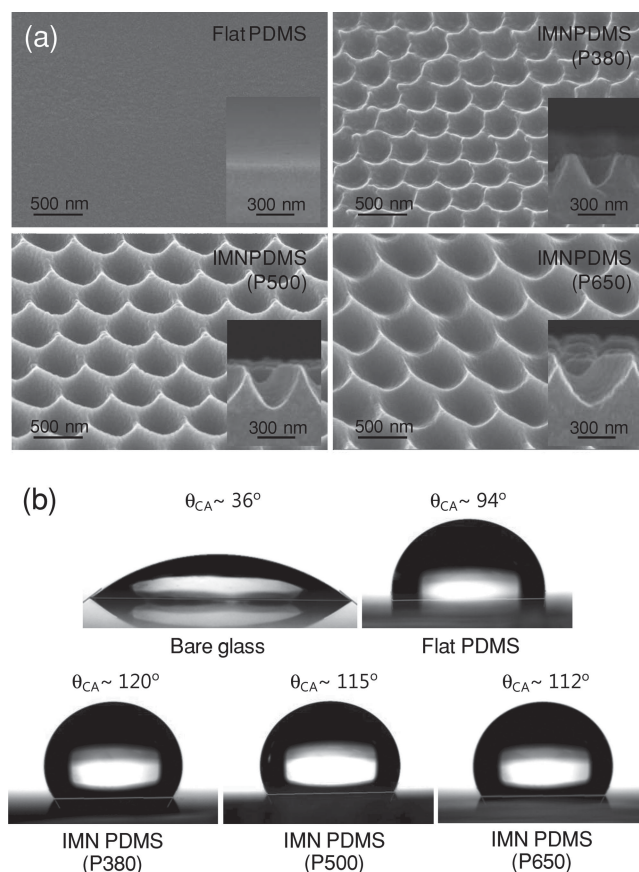


Figure 2. a) 30°-tilted oblique- and side-view SEM images of the flat PDMS film and IMN PDMS films with different periods (*P*) of 380, 500, and 650 nm and b) photographs of a water droplet on the corresponding samples. For the bare glass substrate, the photograph of a water droplet is also shown in (b). θ_{CA} is a water contact angle.

s-PDMS film, as can be seen in the SEM images of Figure S1 in the Supporting Information. The results show that the *h*-PDMS is required to prevent deformation and distortion of the nanoscale patterns. As shown in Figure 2b, the flat PDMS film exhibited a hydrophobic behavior, i.e., a water contact angle (θ_{CA}) of $\approx 94^\circ$, while the bare glass substrate was hydrophilic ($\theta_{CA} = 36^\circ$). For the IMN PDMS films, the hydrophobicity was enhanced with θ_{CA} values of $\approx 120^\circ$, 115° , and 112° for periods of 380, 500, and 650 nm, respectively. This effect is attributed to the increased roughness on the surface of PDMS films, which can be explained by the Cassie-Baxter theory.^[25] These θ_{CA} values are lower than those (i.e., $\theta_{CA} > 150^\circ$, superhydrophobicity) in previous work.^[25–28] As shown in Figure S2 (Supporting Information), however, it can be observed that the sand particles on the surface of IMN PDMS film with a period of 380 nm (i.e., $\theta_{CA} \approx 120^\circ$) were clearly washed by the rolling-down water droplets. Thus, this hydrophobic surface can lead to the removal of dust particles and surface contaminants on the device, i.e., self-cleaning.^[24,26]

Figure 3a shows the measured total transmittance spectra of the flat PDMS film and the IMN PDMS films with periods of 380, 500, and 650 nm laminated on glass substrates. For comparison, the total transmittance spectrum of the bare glass substrate is also shown in Figure 3a. The photograph (left) and 30°-tilted oblique-view low-magnification SEM image (right)

of the IMN PDMS film with a period of 380 nm laminated on glass substrate (i.e., IMN PDMS (P380)/glass) are shown in the insets of Figure 3a. As can be seen in Figure 3a, the bare glass substrate had an average transmission (T_{avg}) of $\approx 90.2\%$ in the wavelength region of 350–800 nm. On the contrary, the flat PDMS film laminated on glass substrate (i.e., flat PDMS/glass) slightly increased the transmission, indicating a T_{avg} of $\approx 91.5\%$. This result is due to the graded refractive index distribution between air and the soda lime glass ($n \approx 1.53$) substrate via the PDMS ($n \approx 1.43$) (see Figure S3a, Supporting Information). For the IMN PDMS/glass samples, the low total transmittance region of $<90\%$ was shifted towards the longer wavelengths with increasing the period. This trend may be caused by diffraction losses at wavelengths shorter than the period due to higher order diffracted waves.^[29,30] However, the IMN PDMS (P380)/glass exhibited a total transmittance higher than 90% over a wide wavelength range of 400–800 nm, indicating a T_{avg} of $\approx 93.8\%$. This value is higher than those of the other samples ($T_{avg} \approx 89.2\%$ for 500 nm of period and $T_{avg} \approx 87.7\%$ for 650 nm) as well as the bare glass substrate and flat PDMS/glass. This behavior can be explained by the fact that the inverted moth-eye patterned nanostructures with periods smaller than the incident light wavelength can more effectively reduce the surface reflection due to a continuous linear gradient in effective refractive index between air and the PDMS (see Figure S3a,

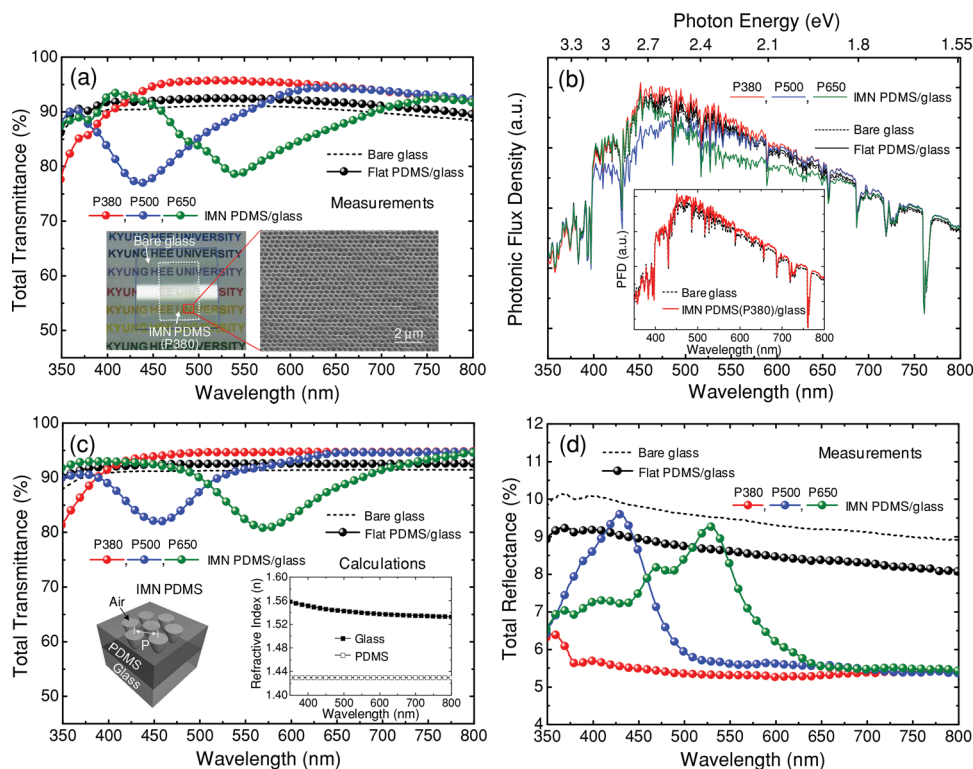


Figure 3. a) Measured total transmittance spectra of the flat PDMS film and the IMN PDMS films with $P = 380, 500,$ and 650 nm laminated on glass substrates. Photograph (left) and 30°-tilted oblique-view low-magnification SEM image (right) of the IMN PDMS (P380) laminated on a glass substrate are shown in the insets of (a). b) Spectral distributions of the PFD for the corresponding samples. c) Calculated total transmittance spectra of the corresponding samples using the RCWA method. The scale-modified simulation model (left) and refractive indices (right) of glass and PDMS used in these calculations are also shown in the insets of (c). d) Measured total reflectance spectra of the corresponding samples. For comparison, the total transmittance and reflectance spectra of the bare glass substrate are also shown in (a,d), respectively.

Supporting Information) as well as the only allowed zeroth-order transmitted wave,^[29–31] which enhances the transmission. Also, these AR characteristics can be observed in the calculated electric field (E-field) intensity distributions (see Figure S3b, Supporting Information). For the bare glass substrate, the E-field intensity is high in the air region because of its strong surface reflection. On the other hand, for the IMN PDMS film, there exists a relatively weak E-field intensity in the air region (stronger E-field intensity in the PDMS film) due to its AR properties.

To investigate the influence of the transmission properties of IMN PDMS films as AR layers on the solar cell performance, the solar weighted transmittance (SWT), which is the ratio of the usable photons transmitted to the total usable photons, was explored. The SWT can be evaluated by normalizing the transmittance spectra with the solar spectral photon flux (i.e., AM1.5G spectrum photonic flux)^[32] integrated over a wavelength range of 350–800 nm.^[33] The SWT is given by

$$\text{SWT} = \frac{\int I_s(\lambda)T(\lambda)d\lambda}{\int I_s(\lambda)d\lambda} \quad (1)$$

where $I_s(\lambda)$ is a spectral irradiance (i.e., AM1.5G) and $T(\lambda)$ is the total transmittance in Figure 3a. As expected, for IMN PDMS (P380)/glass, the SWT value of $\approx 94.2\%$ was higher than those for the bare glass substrate (SWT $\approx 90.3\%$) and other samples (SWT ≈ 91.7 for the flat PDMS/glass and SWT ≈ 90.5 and 87.7% for the IMN PDMS/glass with the periods of 500 and 650 nm, respectively).

These transmission characteristics can be also observed by the calculation of the photonic flux density (PFD) which is the number of photons transmitted across the IMN PDMS/glass.^[34] The PFD is defined as

$$\text{PFD}(\nu) = \frac{I_s T}{h\nu} \quad (2)$$

where I_s is a spectral irradiance (i.e., AM1.5G) and T is the total transmittance in Figure 3a, and $h\nu$ is a photon energy. Figure 3b shows the spectral distributions of the PFD for the corresponding samples. The IMN PDMS (P380)/glass exhibited a higher PFD spectral distribution, particularly at wavelengths of 430–620 nm, which is a range of high solar spectral photonic flux intensity, than other samples. Compared with the bare glass substrate, it also had the highest PFD spectral distribution over a wavelength region of 400–800 nm, as can be seen in the inset of Figure 3b.

For analysis of IMN PDMS films laminated on glass substrates, optical transmittance calculations were also performed using the RCWA simulation. Figure 3c shows the calculated total transmittance spectra of the corresponding samples. The scale-modified simulation model (left) and refractive indices (right) of glass and PDMS used in these calculations are shown in the insets of Figure 3c. As in Figure 3c, the calculated transmittance results showed similar trends to the measured data in Figure 3a, indicating SWT values of ≈ 94.4 , 91, and 88% for IMN PDMS/glass samples at periods of 380, 500, and 650 nm, respectively, (i.e., SWT ≈ 90.8 and 92.3% for the bare glass substrate and flat PDMS/glass, respectively) in the wavelength

region of 350–800 nm. For the effect of the period of IMN on the transmission of IMN PDMS/glass, further details can be found in Figure S4 (Supporting Information). From the simulated results, at periods of < 300 nm, the IMN PDMS film can effectively enhance the transmission of a glass substrate over a wide wavelength range of 350–800 nm, exhibiting the T_{avg} and SWT values of ≈ 94.6 and 94.7% , respectively. To compare with IMN PDMS/glass, optical transmission properties of moth-eye nanopatterned (MN) PDMS films with conical subwavelength grating arrays on glass substrates were also theoretically studied, as in Figure S5 (Supporting Information). Between the total transmittance spectra of both the samples, although there exists a difference at wavelengths of 350–800 nm, they show similar T_{avg} and SWT values.

For all the samples, the total reflectance spectra were also investigated, as shown in Figure 3d. The reflection properties showed trends similar to those of the transmission characteristics in Figure 3a. The PDMS/glass samples exhibited a lower reflectivity than that of the bare glass substrate in the wavelength range of 350–800 nm. Clearly, the IMN PDMS (P380)/glass had a much lower solar weighted reflectance (SWR), which can be similarly estimated from the SWT formula in Equation (1) by replacing the transmittance (T) with the reflectance (R),^[33] of $\approx 5.5\%$ in the wavelength range of 350–800 nm compared to the bare glass substrate (SWR $\approx 9.4\%$) as well as other samples (SWR $\approx 8.6\%$ for the flat PDMS/glass and SWR ≈ 6.3 and 6.8% for the IMN PDMS/glass samples with the periods of 500 and 650 nm, respectively). This high transmission (or AR) property can be confirmed by the photograph of the inset of Figure 3a. For the bare glass substrate (blue-dashed box), the characters underneath it are difficult to discern because of strongly reflected white light at the surface. For a period of 380 nm, however, the IMN PDMS film (white-dashed box) laminated on glass substrate showed improved readability, with only modest effects of reflection. The SEM image in Figure 3a also illustrates that the inverted moth-eye nanopatterns are very uniform over a large area. Overall, the observation suggests that IMN PDMS films with periods of 380 nm can improve the PCE of OSCs by enhancing the light capture in the active layer.

Figure 4 shows the SWT of measured specular transmittance spectra for the bare glass substrate and the IMN PDMS (P380)/glass as a function of incident light angle (θ_i) for un-polarized light in the wavelength (λ) range of 350–800 nm. The SWT of calculated total transmittance spectra for the corresponding samples is also shown in the inset of Figure 4. For both the samples, as the θ_i increased, the SWT values decreased. However, the IMN PDMS (P380)/glass exhibited higher SWT values than those of the bare glass substrate at $\theta_i = 10\text{--}70^\circ$, which indicates an average SWT of $\approx 83.9\%$ at $\theta_i = 10\text{--}70^\circ$ (cf., average SWT $\approx 82.2\%$ for the bare glass substrate). In the RCWA calculations, for the IMN PDMS (P380)/glass, the SWT values were higher and exhibited less angle-dependent transmittance characteristics compared to the bare glass substrate in a wide θ_i range of $10\text{--}70^\circ$.

The effect of IMN PDMS/glass on the PCE of encapsulated OSCs was investigated. IMN PDMS films with different periods as AR layers were laminated on the glass substrate of the OSC module consisting of four active (PBDTTT-C:PCBM)

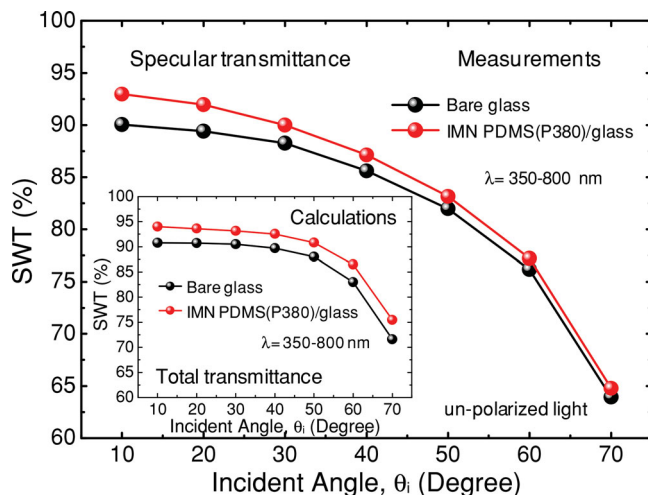


Figure 4. SWT of measured specular transmittance spectra for the bare glass substrate and the IMN PDMS (P380)/glass as a function of incident light angle (θ) for un-polarized light at $\lambda = 350\text{--}800$ nm. The SWT of calculated total transmittance spectra for the corresponding samples is shown in the inset.

devices (see Figure S6, Supporting Information). **Figure 5a** shows the measured current density–voltage (J – V) curves and **Figure 5b** shows the external quantum efficiency (EQE) vs wavelength of the encapsulated OSCs (PBDTTT-C:PCBM) for the bare glass substrate and the IMN PDMS (P380)/glass. **Figure 5c** shows the PCE vs elapsed time for the encapsulated OSC (PBDTTT-C:PCBM) with the IMN PDMS (P380)/glass. A schematic diagram of the OSC structure employed with the AR IMN PDMS film is shown in the inset of **Figure 5a**. The measured device characteristics (open circuit voltage, V_{oc} ; short circuit current density, J_{sc} ; fill factor, FF; PCE) of the encapsulated OSCs for the bare glass substrate and the AR IMN PDMS/glass with different periods are summarized in **Table 1**. Clearly, the IMN PDMS film enhanced the J_{sc} , and thus improved the PCE of OSCs due to its AR property. For the case of IMN PDMS (P380)/glass, the increased J_{sc} of 19.74 mA cm^{-2} was obtained compared to the OSC with the bare glass substrate ($J_{sc} = 17.25\text{ mA cm}^{-2}$), leading to the resultant J_{sc} enhancement percentage of $\approx 14.5\%$. This means that the IMN PDMS film on the glass substrate can enhance the light capture in the active layer of encapsulated OSCs due to reduced surface reflection caused by the gradient effective refractive index profile between air and the PDMS/glass via inverted moth-eye nanostructures. On the other hand, the V_{oc} had no significant difference while the FF was slightly increased from 42.5% for the OSC with the bare glass substrate to 44.84% for the OSC with the AR IMN PDMS (P380)/glass. This variation in FF may be within the noise and sample variability in the measurements. As a result, by laminating the AR IMN PDMS (P380) film on the glass substrate of the encapsulated OSC, the higher PCE of 6.19% was achieved compared to the OSC with the bare glass substrate (PCE = 5.16%) mainly due to enhanced J_{sc} . As shown in **Figure 5b**, the use of the AR IMN PDMS film also improved the EQE spectrum of the OSC over a wide wavelength region of 350–800 nm. This observation is consistent with the reflectance spectrum, which indicates broadband AR properties for the IMN PDMS

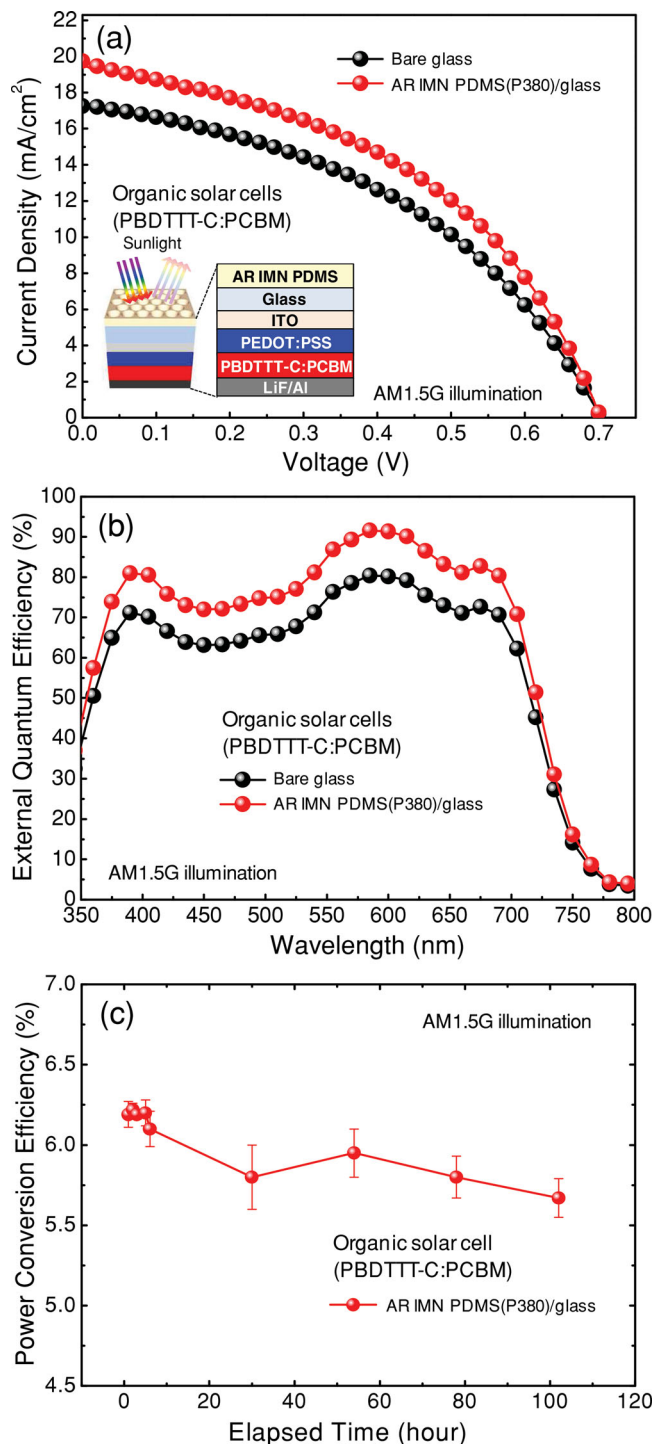


Figure 5. a) Measured J – V curves and b) EQE spectra of the encapsulated OSCs (PBDTTT-C:PCBM) for the bare glass substrate and the AR IMN PDMS (P380)/glass. c) PCE vs elapsed time of the encapsulated OSC (PBDTTT-C:PCBM) with the AR IMN PDMS (P380)/glass. The schematic diagram of the OSC structure employed with the AR IMN PDMS film is shown in the inset of (a).

(P380)/glass, as can be seen in **Figure 3d**. For the OSCs, the device stability was also investigated for 5 days. As can be seen in **Figure 5c**, after 1 day, the device performance was gradually

Table 1. Device characteristics of encapsulated OSCs (PBDDTTT-C:PCBM) for the bare glass substrate and the AR IMN PDMS/glass with different periods.

OSC	V_{oc} [V]	J_{sc} [mA cm ⁻²]	FF [%]	PCE [%]
Bare glass	0.70	17.25	42.75	5.16
AR IMN PDMS (P380)	0.70	19.74	44.84	6.19
AR IMN PDMS (P500)	0.70	18.03	43.44	5.48
AR IMN PDMS (P650)	0.70	17.61	45.80	5.64

degraded due to the poly(3,4-ethylenedioxythiophene):poly(styrenesulfonate) (PEDOT:PSS) acidic layer (HTL) and easily oxidized aluminum (Al) top electrode. Thus, the OSC devices can be damaged by elapsing time and ambient conditions. To avoid the accelerating degradation of device performance, it should be equipped with a desirable encapsulation system. Nevertheless, the PCE of the encapsulated OSC with the AR IMN PDMS (P380)/glass was maintained by 5.67% for 5 days, exhibiting the PCE keeping percentage of $\approx 91.6\%$ compared to its initial value (i.e., PCE = 6.19%). It is important to note that the AR PDMS film with inverted moth-eye nanopatterns can be applied to various other solar cells that use transparent substrates such as glasses, plastics, polymers, and quartzes.

3. Conclusions

AR PDMS films based on inverted moth-eye nanopatterns on one side, fabricated by soft imprint lithography, can improve the PCE of OSCs by enhancing the light capture in their active layer. IMN PDMS films with periods of 380 nm exhibited a hydrophobic property with $\theta_{CA} \approx 120^\circ$. Furthermore, by laminating the IMN PDMS film with a period of 380 nm on glass, higher SWT of $\approx 94.2\%$ and lower SWR $\approx 5.5\%$ were obtained compared to bare glass substrates (SWT $\approx 90.3\%$ and SWR $\approx 9.4\%$). The use of the IMN PDMS film as an AR layer on a glass substrate in an encapsulated OSC (PBDDTTT-C:PCBM) increased the PCE by 6.19% due to the improved J_{sc} of 19.74 mA cm⁻² (PCE = 5.16% and J_{sc} = 17.25 mA cm⁻² for the encapsulated OSC with bare glass substrate). These results suggest that highly transparent nanostructured PDMS films with wide-angle broadband AR properties and self-cleaning properties could be useful in high-performance OSC applications.

4. Experimental Section

Preparation of Si Masters: To form periodic nanopatterns with 2D hexagonal symmetry, photoresist (PR) was spin-coated on Si substrates. Prebaking on a hot plate was carried out at 90 °C for 90 s. The PR was exposed twice with 60° sample rotation between exposures by the interference of two laser beams using a 363.8 nm Ar ion laser. The period (P) of the PR nanopatterns is given by the well-known equation of $P = \lambda / (2 \sin \theta)$, where λ is the laser source wavelength and θ is the angle between the two beams. Thus, the period can be easily controlled by varying the θ , which is adjusted by rotating the rotation stage. After developing, the samples were etched by an inductively coupled plasma etching in SiCl₄ plasma until the removal of PR nanopatterns on the Si

substrate was complete, thus creating the moth-eye nanostructures with a conical shape. For the fabrication of Si masters, further details can be found in our previous work.^[35]

Fabrication of IMN PDMS Films: The IMN PDMS films were fabricated by Si masters with 2D periodic hexagonal moth-eye nanopatterns. A *h*-PDMS solution was prepared by mixing the trimethylsiloxyterminated vinylmethylsiloxane-dimethylsiloxane (VDT-731; Gelest, Inc.) and methylhydrosiloxane-dimethylsiloxane (HMS-301; Gelest, Inc.) copolymers. The *h*-PDMS solution was spin-casted onto the Si master, and then cured at a temperature of 75 °C for 25 min. The *s*-PDMS solution was prepared by Sylgard 184 (Dow Corning Co.) which consists of a silicone "T-resin" cross-linked by a mixture of vinyl-terminated PDMS and trimethylsiloxyterminated poly(methylhydro-siloxane) polymers. Further details can be found in our previous report.^[36] After coating the *h*-PDMS, the *s*-PDMS solution was poured on the *h*-PDMS/Si master, and then cured at 75 °C for 2 h. Finally, the PDMS (*h*-PDMS/*s*-PDMS) film was peeled off, to yield an elastomeric PDMS film with inverted moth-eye nanostructures.

Preparation of OSCs and Characterization: Indium tin oxide (ITO)-coated soda lime glass substrates (13Ω/square, Samsung Corning Corp.) were cleaned with detergent, ultrasonicated in de-ionized water, acetone and isopropyl alcohol, and subsequently dried in an oven for 3 h. The substrates were treated with UV/ozone (for 10 min) to improve the wettability of the PEDOT:PSS buffer solution. As-received PEDOT:PSS solution (Clevios P VP Al 4083) was passed through a 0.45 μm PTFE filter and then spin-casted on patterned ITO/glass substrates at 4000 rpm for 30 s. The substrates were then dried for 15 min at 120 °C on a hotplate (film thickness of ≈ 30 nm) and moved into a glove-box for spin-casting the photoactive layer. Poly[(4,8-bis-(2-ethylhexyloxy)-benzo[1,2-*b*:4,5-*b'*]dithiophene)-2,6-diyl-alt-(4-(2-ethylhexanoyl)-thieno[3,4-*b*]thiophene)-2,6-diyl] (PBDDTTT-C, Solarmer Materials):phenyl-C₆₁-butyric acid methyl ester (PC₆₁BM, Nano-C) (1:1.5, weight ratio) was dissolved in a 1,2-dichlorobenzene:1,8-diiodooctane (97:3, v/v) solvent with a total concentration of 25 mg mL⁻¹ for the active layer. The 1,2-dichlorobenzene solution containing PBDDTTT-C (10 mg mL⁻¹) with PC₆₁BM (15 mg mL⁻¹) was stirred for 1 day at 40 °C into the above solution. All solutions were filtered to remove insoluble impurities using a 0.45 μm PTFE filter before spin-coating. The photoactive layer of PBDDTTT-C:PC₆₁BM was deposited by spin-coating at 1000 rpm for 20 s on top of the PEDOT:PSS buffer layer. The thickness of the photoactive films was estimated to be around 80 nm. Samples were then loaded into a vacuum thermal evaporation system (SPECTROS, Kurt J. Lesker), and 0.7 nm of LiF and 100 nm of Al were deposited using a shadow mask. The J - V curves were measured with a Keithley 2400 source measurement unit under illuminated conditions at an intensity of 100 mW cm⁻² using a 1 kW Oriel solar simulator with an air mass 1.5 global (AM 1.5G) filter. For accurate measurements, the light intensity was calibrated using a radiant power meter and reference silicon solar cells certified by the National Renewable Energy Laboratory (PVM85 with a BK7 window, PVM188 with a KG5 color-filtered window). The EQE spectra were measured by using a lock-in amplifier (SR830, Stanford Research Systems) under short circuit condition while the devices were illuminated by a monochromatic light from a xenon lamp passing through a monochromator (SpectraPro-2150i, Acton Research Corporation).

Characterized Instrumentation: The surface morphologies and patterned profiles of the inverted moth-eye nanostructures on PDMS were observed by using an SEM (LEO SUPRA 55, Carl Zeiss). The optical total transmittance and reflectance properties were measured by using a UV-vis-NIR spectrophotometer (Cary 5000, Varian) with an integrating sphere. For angle-dependent transmittance measurements, spectroscopic ellipsometry (V-VASE, J. A. Woollam Co. Inc.) was used at incident angles of 10–70° in specular mode for un-polarized light. The water contact angles were measured and averaged at three different positions on the surface of samples by using a contact angle measurement system (Phoenix-300, SEO Co., Ltd.).

Theoretical Modeling and Calculation: Optical transmittance calculations of the IMN PDMS films on glass substrate were performed using a commercial software package (DiffRACTMOD 3.1, Rsoft Design

Group).^[37] To design the theoretical models, inverted moth-eye nanostructures on PDMS films were represented in the Cartesian coordinate system by a scalar-valued function of three variables, $f(x,y,z)$, (see Figure S4, Supporting Information). We assumed that the un-polarized incident light entered from air into the structure at incident angles of 0–70° and the thicknesses of PDMS film and glass substrate were set to 250 and 500 μm , respectively.

Supporting Information

Supporting Information is available from the Wiley Online Library or from the author.

Acknowledgements

J.W.L. and S.K. contributed equally to this work. This research was supported by Basic Science Research Program through the National Research Foundation of Korea (NRF) funded by the Ministry of Science, ICT and Future Planning (No. 2013–068407) and the National Research Foundation (NRF) grant funded by the Korean government (Ministry of Science, ICT & Future Planning, MSIP) through the Active Polymer Center for Pattern Integration (APCPI) (2007–0056091).

Received: August 29, 2013

Revised: December 19, 2013

Published online: February 3, 2014

- [1] J. You, L. Dou, K. Yoshimura, T. Kato, K. Ohya, T. Moriarty, K. Emery, C. C. Chen, J. Gao, G. Li, Y. Yang, *Nat. Commun.* **2013**, *4*, 1446.
- [2] S. I. Na, S. S. Kim, J. Jo, S. H. Oh, J. Kim, D. Y. Kim, *Adv. Funct. Mater.* **2008**, *18*, 3956.
- [3] Y. Zhou, C. Fuentes-Hernandez, J. W. Shim, T. M. Khan, B. Kippelen, *Energy Environ. Sci.* **2012**, *5*, 9827.
- [4] Heliateck, <http://www.heliateck.com>, (accessed June 2013).
- [5] M. A. Green, K. Emery, Y. Hishikawa, W. Warta, E. D. Dunlop, *Prog. Photovolt. Res. Appl.* **2013**, *21*, 1.
- [6] S. Kim, J. H. Koh, J. H. Kim, E. Kim, *J. Nanosci. Nanotechnol.* **2013**, *13*, 2632.
- [7] J. K. Koh, J. Kim, B. Kim, J. H. Kim, E. Kim, *Adv. Mater.* **2011**, *23*, 1641.
- [8] J. Kim, J. K. Koh, B. Kim, S. H. Ahn, H. Ahn, D. Y. Ryu, J. H. Kim, E. Kim, *Adv. Funct. Mater.* **2011**, *21*, 4633.
- [9] J. Kim, J. K. Koh, B. Kim, J. H. Kim, E. Kim, *Angew. Chem. Int. Ed.* **2012**, *51*, 6864.
- [10] Y. Kim, Y. Kim, S. Kim, E. Kim, *ACS Nano* **2010**, *4*, 5277.
- [11] Y. Liang, Z. Xu, J. Xia, S. T. Tsai, Y. Wu, G. Li, C. Ray, L. Yu, *Adv. Mater.* **2010**, *22*, E135.
- [12] S. G. Lee, D. Y. Lee, H. S. Lim, D. H. Lee, S. Lee, K. Cho, *Adv. Mater.* **2010**, *22*, 5013.
- [13] S. Y. Chuang, C. C. Yu, H. L. Chen, W. F. Su, C. W. Chen, *Sol. Energy Mater. Sol. Cells* **2011**, *95*, 2141.
- [14] K. Choi, S. H. Park, Y. M. Song, Y. T. Lee, C. K. Hwangbo, H. Yang, H. S. Lee, *Adv. Mater.* **2010**, *22*, 3713.
- [15] D. H. Ko, J. R. Tumbleston, K. J. Henderson, L. E. Euliss, J. M. DeSimone, R. Lopez, E. T. Samulski, *Soft Matter* **2011**, *7*, 6404.
- [16] Y.-N. Xia, G.-M. Whitesides, *Annu. Rev. Mater. Sci.* **1998**, *28*, 153.
- [17] T. Bhuvana, B. Kim, X. Yang, H. Shin, E. Kim, *Angew. Chem. Int. Ed.* **2013**, *52*, 1180.
- [18] Y. M. Song, Y. Xie, V. Malyarchuk, J. Xiao, I. Jung, K. J. Choi, Z. Liu, H. Park, C. Lu, R. H. Kim, R. Li, K. B. Crozier, Y. Huang, J. A. Rogers, *Nature* **2013**, *497*, 95.
- [19] J. Lee, J. Wu, M. Shi, J. Yoon, S. I. Park, M. Li, Z. Liu, Y. Huang, J. A. Rogers, *Adv. Mater.* **2011**, *23*, 986.
- [20] R. H. Kim, D. H. Kim, J. Xiao, B. H. Kim, S. I. Park, B. Panilaitis, R. Ghaffari, J. Yao, M. Li, Z. Liu, V. Malyarchuk, D. G. Kim, A. P. Le, R. G. Nuzzo, D. L. Kaplan, F. G. Omenetto, Y. Huang, Z. Kang, J. A. Rogers, *Nat. Mater.* **2010**, *9*, 929.
- [21] C. D. Sheraw, L. Zhou, J. R. Huang, D. J. Gundlach, T. N. Jackson, M. G. Kane, I. G. Hill, M. S. Hammond, J. Campi, B. K. Greening, J. Francl, J. West, *Appl. Phys. Lett.* **2002**, *80*, 1088.
- [22] J. K. Hyun, C. Ahn, H. Kang, H. J. Kim, J. Park, K. H. Kim, C. W. Ahn, B. J. Kim, S. Jeon, *Small* **2013**, *9*, 369.
- [23] K. Forberich, G. Dennler, M. C. Scharber, K. Hingerl, T. Fromherz, C. J. Brabec, *Thin Solid Films.* **2008**, *516*, 7167.
- [24] R. Blossey, *Nat. Mater.* **2003**, *2*, 301.
- [25] A. D. Tserepi, M. E. Vlachopoulou, E. Gogolides, *Nanotechnology* **2006**, *17*, 3977.
- [26] J. Zhu, C. M. Hsu, Z. Yu, S. Fan, Y. Cui, *Nano Lett.* **2010**, *10*, 1979.
- [27] W. L. Min, B. Jiang, P. Jiang, *Adv. Mater.* **2008**, *20*, 3914.
- [28] W. K. Cho, I. S. Choi, *Adv. Funct. Mater.* **2008**, *18*, 1089.
- [29] Y. M. Song, H. J. Choi, J. S. Yu, Y. T. Lee, *Opt. Express* **2010**, *18*, 13063.
- [30] J. W. Leem, Y. Yeh, J. S. Yu, *Opt. Express* **2012**, *20*, 4056.
- [31] J. W. Leem, Y. M. Song, J. S. Yu, *Opt. Express* **2011**, *19*, A1155.
- [32] NREL's Renewable Resource Data Center. <http://rredc.nrel.gov/solar/spectra/am1.5>, (accessed May 2013).
- [33] H. Cui, S. Pillai, P. Campbell, M. Green, *Sol. Energy Mater. Sol. Cells* **2013**, *109*, 233.
- [34] S. A. Boden, D. M. Bagnall, *Prog. Photovolt. Res. Appl.* **2009**, *17*, 241.
- [35] J. W. Leem, Y. M. Song, Y. T. Lee, J. S. Yu, *Appl. Phys. B* **2010**, *100*, 891.
- [36] K. M. Choi, J. A. Rogers, *J. Am. Chem. Soc.* **2003**, *125*, 4060.
- [37] DiffractMOD, RSoft Design Group. <http://www.rsoftdesign.com>, (accessed January 2013).